

Automatic algorithm to obtain $v \sin i$ values via Fourier Transform in BeSOS database

Martín Solar,^{1,2*} Catalina Arcos,¹ Michel Curé,¹ Ronaldo S. Levenhagen³ and Ignacio Araya⁴

¹*Instituto de Física y Astronomía, Facultad de Ciencias, Universidad de Valparaíso, Gran Bretaña 1111, Valparaíso, Chile*

²*Astronomical Observatory Institute, Faculty of Physics, Adam Mickiewicz University, ul. Słoneczna 36, 60-286 Poznań, Poland*

³*Departamento de Física, Universidade Federal de Sao Paulo, Rua Prof. Artur Riedel, 275, 09972-270, Diadema, SP, Brazil*

⁴*Centro de Investigación DAI_{TA} Lab, Facultad de Estudios Interdisciplinarios, Universidad Mayor, Alonso de Córdova 5495, Santiago, Chile*

Accepted XXX. Received YYY; in original form ZZZ

ABSTRACT

Be stars are found to rotate close to their critical rotation and therefore they are considered as an important laboratory of study for stellar rotation. In this context, we obtain the projected rotational velocity of a sample of classical Be Southern stars in the BeSOS database via Fourier Transform in an automated way for several absorption lines at different epochs. A Gaussian profile is fitted to eight observed photospheric He I lines in order to select automatically the spectral signal given by areas under the curve of 95.45 %, 98.75 % and 99.83 % from the profile to obtain $v \sin i$ via Fourier Transform technique. The values obtained are in global agreement with the literature. Analysing only one line is not enough to set the $v \sin i$ value, depending on the line the value in most cases are underestimated with respect to $\lambda 4471$. When gravity darkening effects are including, apparent values increases by ~ 10 %. The resolution of the instrument PUCHEROS used for BeSOS spectra ($R \sim 17\,000$) constrain a theoretical lower bound possible at $v \sin i \sim 100 \text{ km s}^{-1}$. The procedure has limitations using a linear limb-darkening function with $\varepsilon = 0.6$ for classical Be stars rotating close to the break-up velocity without gravity-darkening corrections, which can't be negligible. Previous works measure $v \sin i$ values using just one spectral line and here we demonstrate that with more lines the results can varies. This could be due to the photospheric distribution of atomic transitions on classical Be stars.

Key words: lines: profile – methods: numerical – methods: statistical – stars: massive – stars: rotation – techniques: spectroscopic

1 INTRODUCTION

The estimation of stellar rotation velocities from spectral line widths dates back to the early work by Abney (1877). Today, there are multiple methods at our disposal to measure the projected rotation velocity ($v \sin i$), but systematic differences among them are still challenging to deal with. Shajn & Struve (1929) suggested a simplified graphical model, without limb-darkening, which turned out to be a standard reference through decades (Collins & Truax 1995). Later, Slettebak published several works (Slettebak & Howard 1955; Slettebak 1954, 1955, 1956) aiming to measure $v \sin i$ using this feature. These works were further revised and a new standard system of rotating velocity stars across the HR diagram was elaborated (Slettebak et al. 1975). These works gave rise to systems of standard stars of rotation velocity, subsequently adopted in calibrations of the full width at half-maximum (FWHM), or even the equivalent width, against $v \sin i$.

Another class of methods, relying on the Fourier transform (FT) of line profiles, to derive $v \sin i$ from the first measured roots, were first proposed by Carroll (1928, 1933); Carroll & Ingram (1933) and are extensively used in the literature (Ilin & Ivanov 1979; Jankov 1995; Reiners & Schmitt 2002; Reiners 2003; Royer 2005; Simón-Díaz et al. 2006; Simón-Díaz & Herrero 2007; Díaz et al. 2011; Ramírez-Agudelo et al. 2013). When compared to Shajn's simple graphical

model, these methods have the advantage of being free of external calibrations and allowing the identification of extra broadening mechanisms and even differential rotation provided the line profiles have a high signal-to-noise (S/N) relation (Gray 1977; Bruning 1981; Reiners & Schmitt 2002). More sophisticated methods of this kind, like that proposed by Díaz et al. (2011), employ the cross-correlation function (CCF) of the profile against a zero-rotation template and apply the FT of the CCF maximum to measure $v \sin i$.

In the present work we intend to apply the classical FT method, specifically to the study of Be stars. Classical Be stars (CBes) are B-type main sequence (MS) stars holding, at least once in their lives, a geometrically thin equatorial disc rotating in a Keplerian way (Rivinius et al. 2013). The nature of the disc formation process is not completely understood, but stellar rotation plus additional mechanisms, are proposed to play an important role (Baade et al. 2016). As CBes rotate close to their critical velocity limit (Porter & Rivinius 2003), the rotation kernel dominates over other broadening mechanisms. Additionally, these stars are generally deformed by rotation, leading to an oblate spheroidal shape. As a result, the temperature and gravity in the surface has a strong dependency with the stellar latitude. Regions closer to the equator have the greater velocities, but are at the same time the coldest ones, so the flux contribution from these regions to the spectrum are lesser than for higher latitudes. This effect is known as gravity-darkening (GD) and was first reported by von Zeipel (1924a,b).

Until today, there is not a variant of the FT method capable of

* E-mail: martin.solar@postgrado.uv.cl

estimating $v \sin i$ and deal with GD at the same time. In a recent work, [Frémat et al. \(2005\)](#) performs a sophisticated analysis among rotating models affected by both gravity-darkening (GD) and rotational distortion, and parent non-rotating counterpart model spectra, to yield “true” $v \sin i$ values, but this analysis does not involve FT’s.

High stellar rotation impacts directly the evolution of stars. As the star rotates near the break-up velocity, its shape becomes oblate and the gas pressure goes down at the equatorial regions. This leads to a decrease in luminosity and a potential increase in its life along the main sequence. Also, the meridional circulation induced by rotation, known as Eddington-Sweet currents, brings the elements formed deep inside the star to its surface, and changing the chemical content of its photosphere ([Maeder & Meynet 2010](#)).

Concerning CBes, helium lines are more dominated by the rotational kernel than other broadening mechanisms such as intrinsic, thermal, turbulent, or Stark, supporting their use. Also, there are essential benefits to using FTs instead of directly comparing an observed line profile with stellar atmosphere models because the line shape is more prominent in the Fourier domain than in the wavelength domain for the reason that includes the whole feature of the spectral signal. Additionally, Gaussian noise is more easily distinguished from the signal ([Smith & Gray 1976](#)). Usually, only the He I $\lambda 4471$ is used to measure $v \sin i$ in CBes because the depth formation is higher than Balmer lines and in this work we use seven more He I photospheric lines for comparison purposes ([Mihalas 1964](#); [O’Mara & Simpson 1972](#); [Neiner et al. 2002](#); [Vinicius et al. 2006](#)). In the case of rapid rotators ($100\text{--}400 \text{ km s}^{-1}$) GD effects given by temperature inhomogeneity on surfaces cause considerable variations in the strength and profile shape of spectral lines on the stellar disc ([Preston et al. 2019](#)). In this work, we use a code by [Levenhagen \(2014\)](#) to calculate line profiles assuming GD, and we estimate the “true” $v \sin i$ values from the interpolation of corrections in temperature, gravity and $v \sin i$ by [Frémat et al. \(2005\)](#).

Multiple works have been done in obtaining the projected rotational velocity in stars, however, in most of them there are no mathematical model that quantify an automatic algorithm to select the signal of an absorption line broadened by Doppler effect due to rotation, and for instance, [Simón-Díaz & Herrero \(2014\)](#) select manually the midwave and continuum of the absorption line to compute the FT. New telescopes and surveys are challenging the form to handle astronomical data ([York et al. 2000](#); [Skrutskie et al. 2006](#); [Gaia Collaboration et al. 2021](#)) and in this work we introduce a procedure using Gaussian fits for the automatic determination of $v \sin i$ based on the FT method since observations growing constantly and it is essential to develop a mechanism capable to deal with this. We performed tests of this algorithm using Monte Carlo (MC) simulations of synthetic spectra affected by different noise levels. The algorithm was applied to “Be Star Observation Survey” (BeSOS) spectra and compared with results from other works.

The outline of the paper is as follows. In Section 2, we present the BeSOS database used in this work. In Section 3, the methodology describes how we propose to obtain $v \sin i$ values using the FT technique. In Section 4, we apply the MC simulations to evaluate the range of applicability of the method. In Section 5, we show the results obtained for BeSOS spectra. Finally, in Sections 6 and 7, the discussion and conclusions are presented, respectively.

2 BESOS DATABASE

In order to test the developed algorithm, we made use of BeSOS spectra ([Arcos et al. 2018](#)), a database which is dedicated to anal-

yse and study the variability of Southern Be stars through optical spectroscopic follow-up. BeSOS contains more than 60 targets (with a limiting visual magnitude of $V=9$) observed between 2012 and 2015, and more than 300 spectra in total with signal-to-noise ratio (SNR) ~ 100 . All spectra are observed with the same instrument, a mid-Resolution ($R \sim 17\,000$) Echelle spectrograph, PUCHEROS ([Vanzi et al. 2012](#)) covering the visible spectral range ($4260\text{--}7300 \text{ \AA}$) and mounted at the 50cm ESO Telescope in the ObsUC located in Santiago, Chile. The data were processed using the CERES pipeline ([Brahm et al. 2017](#)) and the continuum normalisation was made using IRAF packages ([Tody 1993](#)). For more details, we refer to the main BeSOS paper [Arcos et al. \(2018\)](#) and references therein. The spectra are available to download in the BeSOS website¹. Also, the website provides information about the projected rotational velocity values obtained by fitting rotational convoluted stellar atmosphere models ([Kurucz 1979](#); [Hubeny & Lanz 1995](#)) to the observed line profile He I $\lambda 4471$.

3 METHODOLOGY

A spectral line profile can, in principle, be regarded as the convolution between an intrinsic intensity profile and a rotation kernel which is a function of limb-darkening (LD) coefficients and wavelength shifts $\delta = \alpha/\alpha_L$ ([Gray 2005](#)), where we denote for simplicity $\alpha = \Delta\lambda$ to be the wavelength displacement coordinate and $\alpha_L = \Delta\lambda_L$ to be the limit wavelength range of the line profile. Depending on the polynomial fitting that we choose to reproduce the intensities of a spectrum, we will obtain different rotation profiles ([Kopal 1950](#)). In order to apply this technique to the observed line profiles, the broadening mechanism should be dominated by rotation.

Departing from the most simple polynomial line intensities emerging from all stellar directions (I), i.e. a linear LD law ([Carroll 1933](#); [Carroll & Ingram 1933](#)), and assuming spherical stars and rigid rotation we can write the intensity as follows:

$$I(\cos \theta) = I(1) [1 - \varepsilon (1 - \cos \theta)], \quad (1)$$

where the disc’s centre is at $\cos \theta = 1$ and the limb given by $\cos \theta = 0$, and $\varepsilon \in [0, 1]$ is the LD coefficient. By this way the rotation profile can be written as ([Gray 2005](#)):

$$G(\delta) = c_1 (1 - \delta^2)^{1/2} + c_2 (1 - \delta^2), \quad (2)$$

where the linear coefficients are given by:

$$c_1 = \frac{2}{\pi} \left(\frac{1 - \varepsilon}{1 - \varepsilon/3} \right) \quad \text{and} \quad c_2 = \frac{1}{2} \left(\frac{\varepsilon}{1 - \varepsilon/3} \right). \quad (3)$$

The FT of the rotational profile is treated in deep by [Levenhagen \(2014\)](#) for an analogous problem involving different expressions. A linear expression remains, namely:

$$\begin{aligned} \mathcal{F}(G(\alpha)) &= \int_{-1}^1 G(\alpha) \cos(2\pi\sigma\alpha) d\alpha \\ &= c_1 \frac{J_1(2\pi\sigma)}{2\sigma} + c_2 \frac{1}{\pi^2\sigma^2} \left(\frac{\sin 2\pi\sigma}{2\pi\sigma} - \cos 2\pi\sigma \right), \end{aligned} \quad (4)$$

¹ besos.ifa.uv.cl/

where σ is the Fourier coordinate (in units of cycle/Å) associated to the wavelength α coordinate. Assuming $\varepsilon = 0.6$, the first root of the FT occurs at $\alpha_L \sigma_0 = 0.66$. Dividing this root by the first root of the FT of the observed profile will result in the α_L estimate, which is proportional to $v \sin i$. It is commonly assumed a linear LD coefficient of $\varepsilon = 0.6$ in spectral synthesis routines and stellar rotational calculations and it is worth emphasising the strong dependence of ε with temperature, gravity, metallicity, and wavelength (Wade & Rucinski 1985).

We employ the expression found by Dravins et al. (1990) for the first zero of eq. 4 to derive $v \sin i$ using our automated algorithm. It is a power series of the LD coefficient ε with precision of a unit on the third decimal place:

$$\alpha_L \sigma_0 = 0.610 + 0.612 \varepsilon + 0.027 \varepsilon^2 + 0.012 \varepsilon^3 + 0.004 \varepsilon^4, \quad (5)$$

where $\alpha_L = \Delta \lambda_L = (\lambda_{\text{theo}}/c) v \sin i$ represents the maximum broadening that takes place at the stellar limbs (λ_{theo} is the central wavelength of a He I spectral line) and σ_0 is the first zero of the FT frequency domain. $v \sin i$ values obtained by this method are highly dependent of how noisy and how larger is the selected range (spectral signal window) of the absorption line, in which in order to study this behaviour, we simulate an He I line $\lambda_{\text{theo}} = 4713.14 \text{ \AA}$ considering three different noise levels (from a pseudo-random Normal distribution), $\sigma_{\text{noise}} = 0.001, 0.005$ and 0.01 (dimensionless), and three different theoretical projected rotational velocity values, $\langle v \sin i \rangle_{\text{sim}} = 200, 300$ and 400 km s^{-1} (see Fig. 1).

For the selection of the spectral signal window, a Gaussian profile is fitted to the absorption line starting with initial parameters of an amplitude of 0.025 and a standard deviation computed in a range of $\pm 5 \text{ \AA}$ with respect to λ_{theo} . The best parameters are found using a standard non-linear least squares calculation, and hence, the optimal curve is computed. In this case, the information inside $\pm k \sigma_{\text{fit}}$ (dimensionless) window with respect to λ_{theo} is selected, being σ_{fit} the standard deviation of the optimal Gaussian fit. In this work we use $k = 2.0, 2.5$ and 3.0 . The data outside this window is not considered and is defined as continuum. This procedure computes $v \sin i$ selecting automatically the spectral window region to be used in the FT method in any absorption line (He I for our work). Nevertheless, we still need to quantify the obtained $v \sin i$ value as a function of the quality of the observed absorption line, i.e. noisy spectra can yield significant errors, regardless of the parameters to be obtained. For this reason, in this work we propose five criteria described in Table 1 (The sixth criterion is explained in detail in section 4).

If the line satisfies these five criteria, a $v \sin i$ value is computed by the FT method, otherwise, the data is not utilised. It is expected that as noise increases, the projected rotational velocity obtained should be less reliable and to obtain a correct velocity. The criteria try to generalise a well automatic quantification for any absorption line and it depends from the instrument used. In this work, the construction of simulated line profiles are given by as the same spectra resolution of Pontificia Universidad Catolica High Echelle Resolution Optical Spectrograph (PUCHEROS) and the Fiber-fed Extended Range Optical Spectrograph (FEROS; Kaufer et al. 1999) with wavelength steps of 0.089 \AA/pix and 0.03 \AA/pix , respectively.

For the simulated lines from Fig. 1, the FT was applied to every spectral signal windows and velocities in which the results given by the first zero, represents the rotational speed $\langle v \sin i \rangle_{\text{FT}}$ obtained, showed in Fig. 2. In this figure, it can be noted for all $\langle v \sin i \rangle_{\text{sim}}$, the velocities returned are not equal to the simulated one, specially as σ_{noise} increase. The combination of high projected rotational velocity and high noise level ($\sigma_{\text{noise}} = 0.01$ and $\langle v \sin i \rangle_{\text{sim}} = 400 \text{ km s}^{-1}$)

Criteria	Description
1st criterion: A Gaussian profile is successfully fitted given the initial parameters (see text for initial parameters values).	If the observed line profile is undetectable with respect to the continuum, then the numerical fit it is going to fail at the moment to find the optimal curve.
2nd criterion: An absorption line exists when the fitted Gaussian profile has a peak less than 1 (simulated normalised flux).	An atomic transition must be in absorption to trace the atmospheric surface, and sometimes, this line can be contaminated with information from the disk.
3rd criterion: The centre of the Gaussian fit is not shifted more than $k \sigma_{\text{fit}}$ with respect to λ_{theo} .	In some cases there is no absorption line in λ_{theo} and numerically another transition line close to it is found, as is in the case of He I $\lambda 4471$ and MgII $\lambda 4481$. Also, considering the radial velocity displacement from λ_{theo} , the quantity $k \sigma_{\text{fit}}$ leaves a considerable range of error to find the absorption line.
4th criterion: The standard deviation of the continuum σ_c (dimensionless) is lesser than the amplitude of the Gaussian fit.	The goal of this criterion is differentiate if the continuum is too noisy with respect to the line profile.
5th criterion: The dispersion of the Gaussian fit is higher than 5 times the step of the wavelength λ .	To quantify the quality of the signal, there should be at least 5 bins in one σ_{fit} from the Gaussian fit. This tell us that the line has significantly information inside the Gaussian profile.
6th criterion: The standard deviation of the continuum in observations is lesser than the obtained from MC simulations.	Given 10 000 MC simulations for a grid of simulated σ_{noise} and $\langle v \sin i \rangle_{\text{sim}}$, if the σ_c in observations is lesser than median of the simulated ones for a specific velocity, then the absorption line is considered to measure $v \sin i$.

Table 1. Criteria proposed to check if an observed absorption line is considered as a suitable signal.

gives as result a non-fulfilment of one or more of the required criteria and no FT is computed (line dropped). Additionally to this, for $\langle v \sin i \rangle_{\text{FT}}$ there is no clear pattern for the resulted velocities so far and the numerical procedure described in this section has been defined for a single line as an example and results for multiple velocities and noise levels are described in next section using MC simulations.

4 MONTE CARLO SIMULATIONS

Simulated line profiles rotationally convoluted at different noise levels are generated to obtain $v \sin i$ via FT transform with the aim to evaluate the reliability of the procedure. As a first example we assume that the intrinsic line profile of a star can be model by a Gaussian profile with parameters of dispersion 0.1 and amplitude 0.5, this profile is convoluted with a grid of rotational kernels from 100 to 600 in steps of 10 km s^{-1} . In observations it is usual to obtain systematic variations due to instrumental errors and physical effects, among others. To add random noise to the simulated line profile (intrinsic + rotation) a grid of σ_{noise} is included from 0.001 to 0.1 in steps of 0.001.

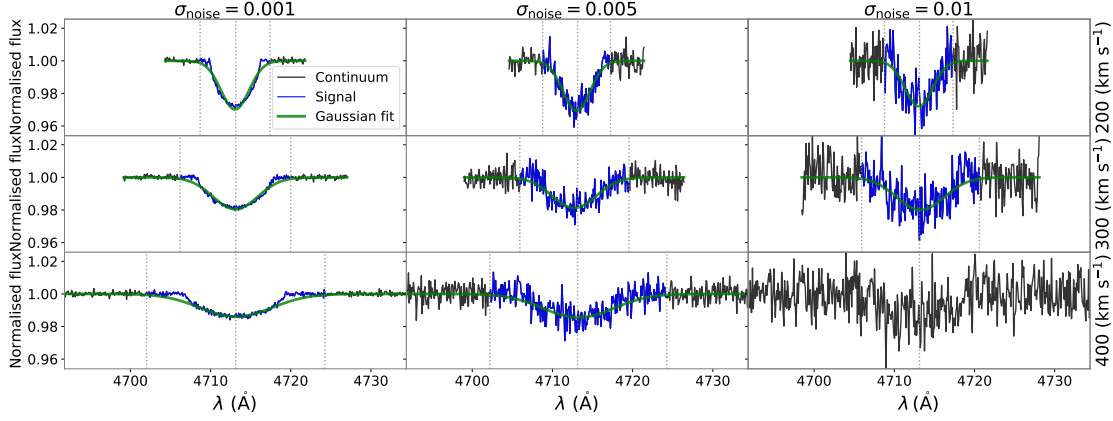


Figure 1. Grid of simulated line profiles with noise and rotational kernels for $2.5 \sigma_{\text{fit}}$. The normalised flux is as a function of the wavelength. The solid green curve represents the best Gaussian fit, the solid blue lines are the selected spectral signal window and the solid black lines represent the continuum. These three sections are indicated by the vertical dotted grey lines. Left panels: $\sigma_{\text{noise}} = 0.001$. Middle panels: $\sigma_{\text{noise}} = 0.005$. Right panels: $\sigma_{\text{noise}} = 0.01$. Top panels: $\langle v \sin i \rangle_{\text{sim}} = 200 \text{ km s}^{-1}$. Middle panels: $\langle v \sin i \rangle_{\text{sim}} = 300 \text{ km s}^{-1}$. Bottom panels: $\langle v \sin i \rangle_{\text{sim}} = 400 \text{ km s}^{-1}$.

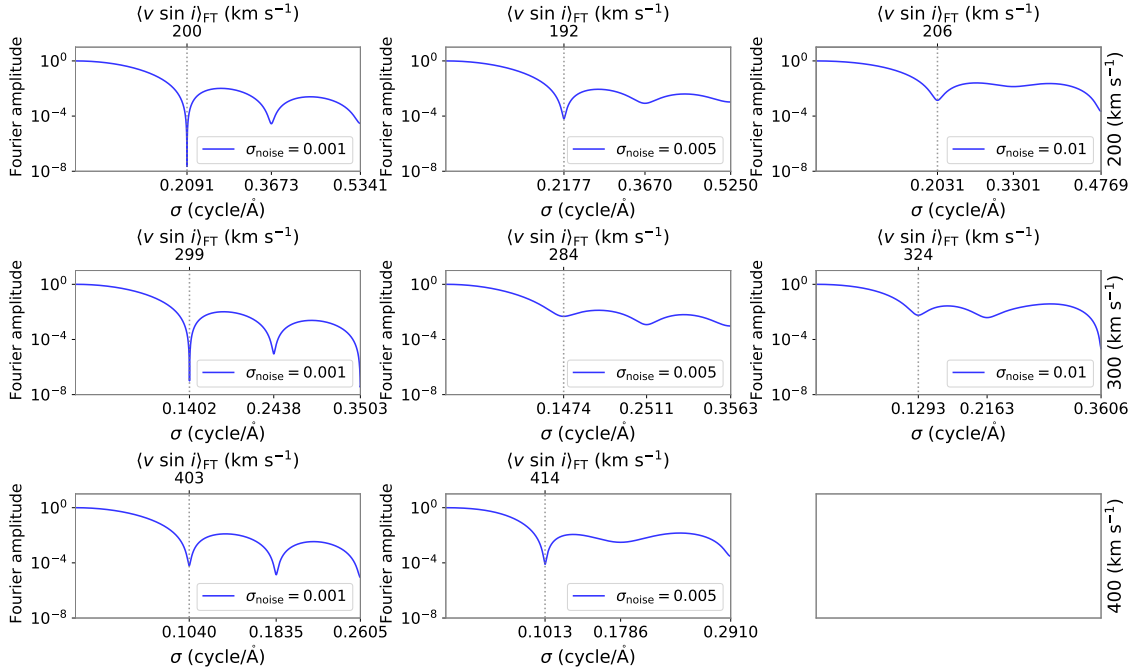


Figure 2. FTs for spectral signal windows of $\pm 2.5 \sigma_{\text{fit}}$ for Fig. 1 represented by a solid blue curve. The subplots show the Fourier amplitude as a function of the Fourier domain σ and their respective conversion of the first zero to the obtained velocity $\langle v \sin i \rangle_{\text{sim}}$, which is denoted by the vertical dotted grey lines. Left panels: $\sigma_{\text{noise}} = 0.001$. Middle panels: $\sigma_{\text{noise}} = 0.005$. Right panels: $\sigma_{\text{noise}} = 0.01$. Top panels: $\langle v \sin i \rangle_{\text{sim}} = 200 \text{ km s}^{-1}$. Middle panels: $\langle v \sin i \rangle_{\text{sim}} = 300 \text{ km s}^{-1}$. Bottom panels: $\langle v \sin i \rangle_{\text{sim}} = 400 \text{ km s}^{-1}$. For the case of $\sigma_{\text{noise}} = 0.01$ and $\langle v \sin i \rangle_{\text{sim}} = 400 \text{ km s}^{-1}$ (right bottom panel), FT is not computed because the line does not satisfy the fifth criterion.

In Fig. 3, for 10 000 MC simulations and a window of $2.5 \sigma_{\text{fit}}$, it is shown the relation between σ_c (see Table 1), fourth criterion and $\langle v \sin i \rangle_{\text{FT}}$ as functions of σ_{noise} for PUCHEROS and FEROS resolutions. The relation 1:1 in left panels evidence that σ_c trace totally σ_{noise} , that is, assuming an observed line profile with Normal noise in the spectrum therefore is possible to obtain the dispersion parameter for the star computing the standard deviation of the

normalised flux. The velocities estimated given by simulated line profiles of $\langle v \sin i \rangle_{\text{sim}} = 300 \text{ km s}^{-1}$ for the whole grid of σ_{noise} are presented in right panels. It can be noted that the $v \sin i$ values decrease from $\sigma_{\text{noise}} > 0.015$ and in $\sigma_{\text{noise}} = 0.023$, when $\Delta 10\%$ of $\langle v \sin i \rangle_{\text{sim}}$ (270 km s^{-1} in this case) is reached, then the velocity yielded is not reliable, given by MC simulations. This critical σ_c (or σ_{noise}) is defined as $\sigma_{c,\text{crit}}$ (or $\sigma_{\text{noise,crit}}$). For the case of

FEROS resolution, the decrease velocities is at higher noise, being $\sigma_{\text{noise}} = 0.024$ when the median of the 10 000 MC is reached for 270 km s⁻¹. In addition, error bars suggest that for FEROS is lower than PUCHEROS. For this reason an instrument with high resolution yields more reliable results.

We adopt this threshold as our last criteria to select “good” lines, the sixth criterion, which yields an extra support to the procedure given our MC simulations and is presented in the last row of Table 1. Figure 4 shows the behaviour of $\sigma_{c,\text{crit}}$ for the grid of simulated $v \sin i$. For high rotators the critical measured noise $\sigma_{c,\text{crit}}$ is lesser than slow rotators and this is because as rotational velocity increases, the magnitude of the signal decreases and is broadened, which makes the observed line harder to detect (same case of $\sigma_{\text{noise}} = 0.01$ and $\langle v \sin i \rangle_{\text{sim}} = 400 \text{ km s}^{-1}$ in Fig. 1).

It is important to mention that for slow rotators, the number of bins within a thin absorption line is insufficient to compute the FT. In the study of Simón-Díaz & Herrero (2014) they concluded that any $v \sin i$ measurement below 40 km s⁻¹ using FT has to be taken as the upper limit (if effects of microturbulence are not included). The data from that work were given by the FIBRE-fed Echelle Spectrograph (FIES) medium and low- resolution with resolutions of $R \sim 23\,000$ and $46\,000$, respectively, both having a spectral dispersion of 0.025 Å/pix. For our case, we use the BeSOS database which has the same bin steps for simulations implemented in this work. In our work, the simulation shows that values below 100 km s⁻¹ and $\sigma_{c,\text{crit}}$ are considered as unreliable results. However, as majority of CBes rotate higher than this velocity this is not a problem and this should be taken account for stars of lower rotation (see Table 2).

5 APPLICATION TO BESOS DATABASE

The procedure was applied to BeSOS database for 64 stars at different epochs with a total of 314 spectra. As we use eight He I absorption lines, in order to visualise the spectra, Fig. 5 shows the procedure implemented to HD157246 for a single epoch using a window of $2.5 \sigma_{\text{fit}}$.

In this figure, seven of eight lines were used to measure $v \sin i$ because in case of $\lambda 4921$, the sixth criterion detect a high level of noise in the continuum. This last case is interpreted by different normalised continuum rates in the left and right sides from the midwave, values of ~ 1 and ~ 0.95 , respectively. Non-radial pulsation and stellar winds for Be stars tend to be the main source of asymmetry, but it is not discarded the influence of other processes such as line blendings with near transitions, differential rotation or even minor physical phenomena such as turbulence. However, we tried to select only helium line profiles that were less affected by asymmetries for our study using the sixth criterion. Simón-Díaz & Herrero (2014) presents a friendly-interactively code that solves this problem selecting the continuum part manually. In Fig. 6, the $v \sin i$ values are represented for HD157246 at four different epochs.

To determine the average per star boxplots for all $\langle v \sin i \rangle_{\text{FT}}$ were computed. This technique consist in obtain the first quartile, the median and the third quartile, and the interquartile range (IQR). Following this, to exclude outliers the 1.5 IQR above and below the third and first quartiles are calculated. The values above or below this range are considered as outliers. As can be noted the dispersion of values is still high; it changes from $200 \text{ km s}^{-1} < v \sin i < 310 \text{ km s}^{-1}$ to $220 \text{ km s}^{-1} < v \sin i < 290 \text{ km s}^{-1}$. Looking for a relation between

the Modified Julian Date² (MJD) and the type of absorption line used in this star, it can be infer that there is no clear relation.

To survey the averaged $v \sin i$ values for windows of $2.0 \sigma_{\text{fit}}$, $2.5 \sigma_{\text{fit}}$ and $3.0 \sigma_{\text{fit}}$, Table 2 shows the results compared to Arcos et al. (2018) as “Arcos+2018” and Frémat et al. (2005) as “Fremat2005” were they calculated $v \sin i$ using synthetic spectra with classical plane parallel non-LTE model atmospheres using apparent fundamental parameters derived from He I 4471 line.

Besides, in Fig. A1 the relation between the $v \sin i$ values obtained by our method (using $k = 2.0, 2.5$ and 3.0) are compared with literature results (Fremat2005 and Arcos+2018).

6 DISCUSSION

6.1 Lower limit of $v \sin i$

PUCHEROS versus FEROS resolutions evidence from Fig. 3 that the capacity of the instrument is a very important feature because the higher the SNR, the smaller is the $v \sin i$ lower limit value that this method delivers. Based on our procedure to obtain the projected rotational velocities for BeSOS database, three stars (HD13876, HD89890 and HD5721) presented a $v \sin i$ lower than 100 km s⁻¹ and therefore their projected rotational speeds are considered equal to 100 km s⁻¹. Sundqvist et al. (2013) and Simón-Díaz & Herrero (2014) claim that, using FT and goodness-of-fit (GOF) methods, it is not possible to derive reliable projected rotation speeds when $v \sin i \lesssim 40 - 50 \text{ km s}^{-1}$.

6.2 He I $\lambda 4471$ line

Having the velocities averaged per line for each star, Fig. 7 shows the behaviour for $\lambda 4471$ He I line versus all the other ones used ($\lambda \lambda 4387, 4713, 4921, 5015, 5047, 5875$ and 6678) for a window of $2.5 \sigma_{\text{fit}}$ and with confidence intervals of 16% – 84%. This absorption line is chosen for comparison reasons since it is essential to analyse how the other lines are approached with respect to $\lambda 4471$ He I line.

Two fits are included in this figure, a linear least square polynomial fit and a 1:1 relation line in order to analyse relations for $v \sin i$ values at different λ_{theo} . Correlation coefficients are included on the insets for each subplot. The $\lambda 4471$ with the $\lambda 4921$ lines are correlated very well with 0.696 and indeed, the 1:1 relation is very similar to the linear fit. Giving that in general, these two lines can be conceived as equal lines. The cases that are relatively well correlated are $\lambda 4471$ versus $\lambda 5015$ and $\lambda 6678$ with the difference that in both cases the velocities are slightly underestimated. For the following samples are $\lambda 4387$ and $\lambda 4713$, in which R^2 are 0.421 and 0.46, respectively. On the other hand, the linear fits, compared to $\lambda 4471$, are underestimated (for $\lambda 4387$) and very similar ($\lambda 4712$).

As a general perspective, there is a trend for the other seven He I lines ($\lambda \lambda 4387, 4713, 4921, 5015, 5047, 5875$ and 6687) to underestimate $v \sin i$ values with respect to the values from $\lambda 4471$. Alternatively, the average per star (same as Table 2) is plotted as a function of the eight $\langle v \sin i \rangle_{\text{line}}$ in Fig. 8 for a window of $2.5 \sigma_{\text{fit}}$ and with confidence intervals of 16% – 84%.

In this figure, the best correlation factor ($R^2 = 0.738$) is for $\lambda 5875$ with respect to $\lambda 4471$. For lower velocities, in average, the values are underestimated and for higher velocities are overestimated, which yields in a fit upper the 1:1 relation. The cases of $\lambda \lambda 4471$ and 5015 gives a squared correlation factor of 0.734 and 0.711, respectively,

² MJD = JD – 2400000.5

Target	$2.0 \sigma_{\text{fit}}$	$2.5 \sigma_{\text{fit}}$	$3.0 \sigma_{\text{fit}}$	N ^o of epochs	Arcos+2018	Fremat2005
HD10144	228 ⁺³¹ ₋₁₃	225 ⁺²⁹ ₋₅₁	225 ⁺⁵⁹ ₋₃₉	2	—	—
HD33328	283 ⁺⁴⁰ ₋₅₀	279 ⁺³² ₋₅₂	292 ⁺²⁵ ₋₃₀	5	287	333
HD35165	213 ⁺⁶³ ₋₂₂	217 ⁺⁴ ₋₉	211 ⁺³⁶ ₋₆₁	7	240	350
HD35411	320 ⁺¹⁰³ ₋₇₆	327 ⁺³⁵ ₋₄₄	325 ⁺⁹⁰ ₋₈₆	5	53	174
HD35439	244 ⁺⁶⁰ ₋₈₂	230 ⁺⁷⁷ ₋₆₈	253 ⁺⁶¹ ₋₆₃	8	266	266
HD37041	149 ⁺³⁰ ₋₄₃	132 ⁺²⁴ ₋₁₆	135 ⁺¹⁹ ₋₁₄	5	140	133
HD37795	190 ⁺²⁷ ₋₃₃	181 ⁺²³ ₋₅₁	188 ⁺⁹⁴ ₋₅₆	9	—	192
HD41335	242 ⁺⁸⁵ ₋₆₄	258 ⁺⁵⁴ ₋₈₆	244 ⁺¹⁰⁰ ₋₇₁	8	330	376
HD42167	199 ⁺⁷⁴ ₋₇₃	203 ⁺⁴⁷ ₋₅₈	190 ⁺⁵² ₋₄₈	6	—	249
HD45725	340 ⁺¹⁰ ₋₁₉	337 ⁺²⁰ ₋₂₀	345 ⁺²⁶ ₋₁₅	2	280	345
HD45910	196 ⁺⁶ ₋₇	131 ⁺⁵⁹ ₋₃₆	137 ⁺⁵⁶ ₋₄₃	6	100	254
HD48917	180 ⁺²⁹ ₋₃₀	167 ⁺⁴⁴ ₋₄₁	191 ⁺²⁴ ₋₅₃	10	200	212
HD50013	231 ⁺³⁴ ₋₅₅	209 ⁺⁴⁹ ₋₃₈	228 ⁺³⁰ ₋₃₇	7	290	244
HD52918	305 ⁺¹⁷ ₋₂₄	303 ⁺⁸ ₋₁₄	309 ⁺¹⁴ ₋₄	2	242	265
HD56014	183 ⁺²⁵ ₋₆₆	199 ⁺⁶ ₋₅₀	129 ⁺⁴⁵ ₋₄₁	2	200	294
HD57150	213 ⁺¹³ ₋₁₈	218 ⁺⁸ ₋₂₃	228 ⁺⁹ ₋₁₉	2	180	190
HD57219	135 ⁺⁰ ₋₀	88 ⁺⁷ ₋₈	84 ⁺¹² ₋₈	4	50	84
HD58715	284 ⁺⁶¹ ₋₈₆	299 ⁺¹¹⁷ ₋₉₄	278 ⁺¹⁶² ₋₆₆	3	—	231
HD60606	249 ⁺²⁹ ₋₃₄	256 ⁺²⁵ ₋₂₄	258 ⁺²³ ₋₂₅	6	250	285
HD63462	238 ⁺⁴⁷ ₋₄₇	279 ⁺²³ ₋₆₉	310 ⁺³⁹ ₋₇₈	3	300	514
HD68980	152 ⁺⁰ ₋₃	127 ⁺¹⁸ ₋₁₁	141 ⁺¹⁰ ₋₆	3	110	152
HD71510	165 ⁺²⁰ ₋₂₈	155 ⁺²⁰ ₋₃₀	155 ⁺¹⁵ ₋₂₃	6	150	154
HD75311	249 ⁺³⁴ ₋₃₉	247 ⁺³⁸ ₋₇₆	256 ⁺²¹ ₋₆₇	2	250	283
HD78764	150 ⁺¹⁹ ₋₃₆	113 ⁺¹² ₋₂₃	122 ⁺¹⁹ ₋₂₃	3	140	120
HD83953	286 ⁺⁶⁹ ₋₂₄	263 ⁺²⁴ ₋₂₂	257 ⁺²⁵ ₋₁₉	1	250	276
HD89080	224 ⁺³¹ ₋₄₅	233 ⁺⁵⁴ ₋₂₉	245 ⁺¹⁸⁷ ₋₆₃	7	—	254
HD89890	130 ⁺⁴ ₋₅₇	92 ⁺⁴⁶ ₋₁	97 ⁺² ₋₂₂	5	26	67
HD91465	286 ⁺¹⁴ ₋₁₉	288 ⁺¹ ₋₂₀	290 ⁺¹⁵ ₋₁₄	6	280	285
HD92938	131 ⁺³⁷ ₋₂₁	121 ⁺⁹ ₋₁₆	122 ⁺¹⁶ ₋₉	7	110	139
HD93563	183 ⁺¹⁰¹ ₋₅₄	194 ⁺⁹⁵ ₋₅₅	183 ⁺⁹¹ ₋₄₈	6	280	275
HD98058	223 ⁺⁵² ₋₂₆	201 ⁺⁷ ₋₉	219 ⁺² ₋₈	3	—	254
HD102776	222 ⁺¹⁶ ₋₄₀	190 ⁺³⁵ ₋₂₅	197 ⁺²⁴ ₋₂₅	5	200	270
HD103192	275 ⁺¹¹ ₋₄₉	275 ⁺³⁴ ₋₄₁	274 ⁺²⁵¹ ₋₉₇	5	—	42
HD105382	171 ⁺¹² ₋₅	183 ⁺¹⁰ ₋₁₀₈	117 ⁺⁶¹ ₋₁₇	5	67	72
HD105435	257 ⁺³⁴ ₋₈₅	245 ⁺³⁵ ₋₆₃	245 ⁺⁴⁶ ₋₅₉	3	250	163
HD107348	234 ⁺²⁸ ₋₅₂	204 ⁺⁴² ₋₃₁	237 ⁺²⁷ ₋₄₃	5	—	237
HD110335	242 ⁺¹⁵ ₋₇₅	214 ⁺³⁴ ₋₂₃	216 ⁺²⁹ ₋₁₃	3	—	—
HD110432	181 ⁺⁵² ₋₃	184 ⁺²² ₋₇	185 ⁺² ₋₂	4	400	419
HD112078	307 ⁺²⁶ ₋₂	303 ⁺¹ ₋₇₅	338 ⁺⁷² ₋₃₄	1	290	327
HD120324	151 ⁺¹³ ₋₂₅	129 ⁺²¹ ₋₃₂	139 ⁺⁸ ₋₁₁	3	110	162
HD124195	135 ⁺³⁹ ₋₃₄	136 ⁺³⁰ ₋₂₆	185 ⁺¹¹ ₋₅₃	2	150	—
HD124367	248 ⁺¹⁶ ₋₁₆	272 ⁺¹⁶ ₋₁	277 ⁺⁵ ₋₁₈	2	260	318
HD124771	188 ⁺¹⁰ ₋₁₅	164 ⁺²¹ ₋₃₅	175 ⁺²⁰ ₋₂₀	2	150	205
HD127972	245 ⁺⁴⁷ ₋₈₄	203 ⁺⁵⁷ ₋₄₆	206 ⁺⁶⁹ ₋₄₇	4	240	326
HD131492	173 ⁺⁴³ ₋₅₄	168 ⁺⁵⁰ ₋₄₅	152 ⁺⁵⁶ ₋₃₁	6	100	192
HD135734	257 ⁺⁷² ₋₈₈	290 ⁺⁴⁴ ₋₁₀₉	276 ⁺⁶² ₋₁₀₀	7	—	282
HD138769	159 ⁺²⁰ ₋₂₁	102 ⁺⁷⁴ ₋₁₆	91 ⁺²⁵ ₋₁₅	5	30	78
HD142983	227 ⁺⁸³ ₋₅₂	238 ⁺⁷⁹ ₋₃₄	250 ⁺⁵³ ₋₁₇	6	370	407
HD143275	204 ⁺⁴⁷ ₋₃₈	184 ⁺²³ ₋₃₂	203 ⁺¹¹ ₋₇	2	257	150
HD148184	157 ⁺²³ ₋₄₅	134 ⁺³⁷ ₋₂₂	159 ⁺³⁰ ₋₃₅	5	150	151
HD157042	310 ⁺⁴⁵ ₋₅₉	299 ⁺⁶⁶ ₋₃₃	303 ⁺⁵² ₋₂₉	5	280	348
HD157246	257 ⁺⁶ ₋₁₉	258 ⁺⁸ ₋₂₁	262 ⁺⁷ ₋₁₇	4	230	230
HD167128	154 ⁺² ₋₁	186 ⁺² ₋₃	203 ⁺² ₋₁	3	50	55
HD205637	225 ⁺⁴⁶ ₋₄₀	247 ⁺²⁶ ₋₆₅	259 ⁺¹¹ ₋₄₃	2	230	238
HD209014	208 ⁺⁵² ₋₂₅	195 ⁺⁸⁰ ₋₄₃	195 ⁺⁹⁵ ₋₃₃	8	—	357
HD209409	254 ⁺⁴⁶ ₋₁₀₅	244 ⁺³⁰ ₋₉₃	240 ⁺⁴¹ ₋₃₂	7	350	282
HD212076	148 ⁺²⁵ ₋₂₁	142 ⁺⁵⁵ ₋₅₄	120 ⁺⁷⁶ ₋₃₀	6	100	103
HD212571	227 ⁺⁴⁸ ₋₇₈	225 ⁺⁴³ ₋₇₃	239 ⁺⁴⁴ ₋₇₉	7	215	233
HD214748	182 ⁺⁴¹ ₋₂₂	185 ⁺²⁸ ₋₄₁	184 ⁺⁴⁵ ₋₂₇	9	—	205
HD217891	222 ⁺³⁰ ₋₅₃	277 ⁺²⁰ ₋₇₁	271 ⁺¹¹¹ ₋₁₁₂	10	90	100
HD219688	225 ⁺²⁴ ₋₂₂	228 ⁺¹⁵ ₋₄₇	230 ⁺⁵ ₋₅₄	4	—	316
HD221507	237 ⁺³ ₋₆	225 ⁺¹⁸ ₋₂₃	221 ⁺⁶ ₋₂₁	10	—	—

Table 2. Projected rotational velocities obtained by our work for windows of $2\sigma_{\text{fit}}$, $2.5\sigma_{\text{fit}}$ and $3\sigma_{\text{fit}}$ (in km s^{-1} ; 2nd, 3rd and 4th columns, respectively) with confidence interval of 16% – 84%. 5th column represents the number of epochs. 6th and 7th columns are $v \sin i$ (in km s^{-1}) values obtained from literature.

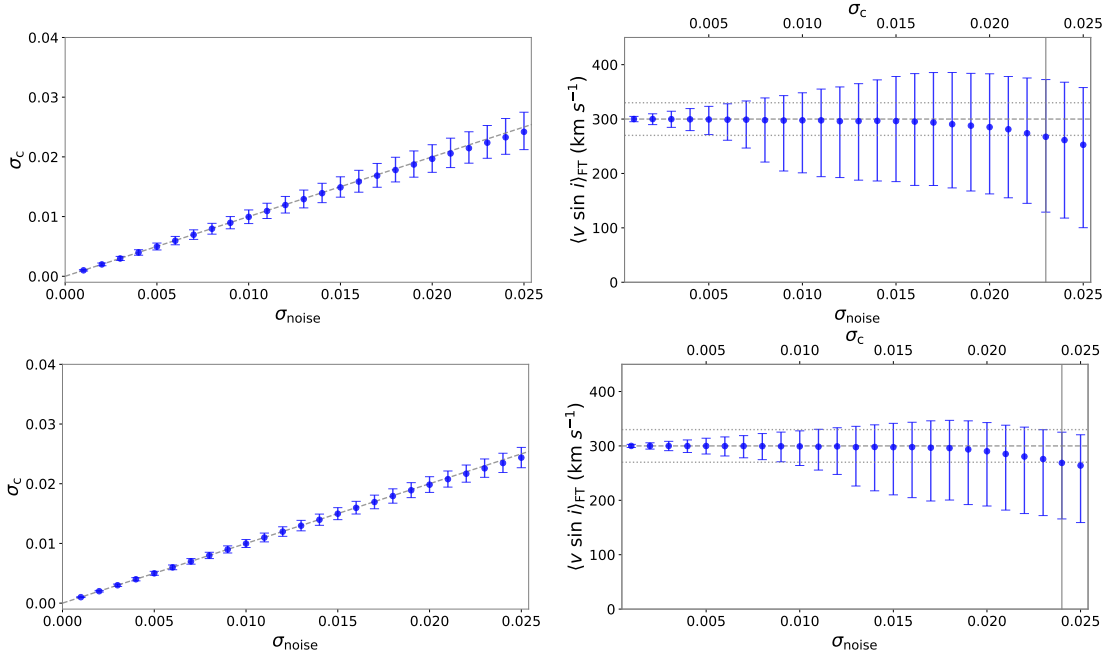


Figure 3. Relation between critical σ_{noise} and σ_c for $2.5\sigma_{\text{fit}}$, for 10 000 MC simulations, and with confidence intervals of 95% (error bars from 2.5% to 97.5%). Left panel: Standard deviation of the continuum as a function of the simulated noise added (blue dots). The 1:1 relation is represented by a dotted grey line. Right panel: Median of $\langle v \sin i \rangle_{\text{FT}}$ as a function of $\sigma_{\text{noise}} = \sigma_c$ (blue dots). The horizontal dashed grey line represents $\langle v \sin i \rangle_{\text{sim}} = 300 \text{ km s}^{-1}$ and the dotted grey dotted lines are $300 \pm 30 \text{ km s}^{-1}$. The vertical dotted grey line indicate $\sigma_{c,\text{crit}}$. Top panels are simulations performed using PUCHEROS resolution and bottom panels for FEROS resolution.

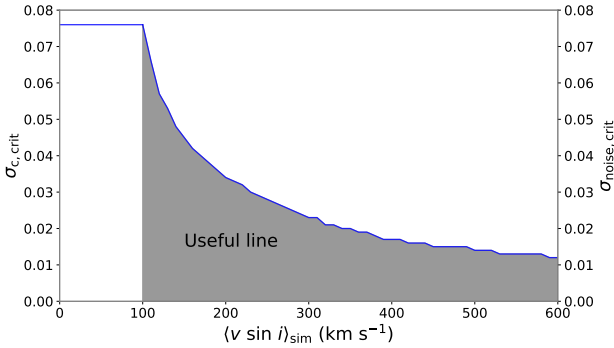


Figure 4. Critical standard deviation of the continuum for observations ($\sigma_{c,\text{crit}}$) or simulations ($\sigma_{\text{noise,crit}}$) as a function of $v \sin i$ via FT (solid blue curve). We notice that these values were obtained for a $\Delta\lambda = 0.089 \text{ \AA}/\text{pix}$ (PUCHEROS resolution). Values below 100 km s^{-1} are unreliable.

with the difference that now the fits are underestimated with respect to the 1:1 relation. The same happens with $\lambda\lambda 4387, 4921$ and 6687 but with lower correlation factors. The other sample that overestimate with respect to $\langle v \sin i \rangle_{\text{final}}$ is the $\lambda 4713$ line with a good correlation. The scenario given by $\lambda 5047$ with a squared degree of correlation factor of 0.36 and a fit that underestimate significantly the velocities. As a general perspective, the average of velocities obtained using our method, in comparison for $\langle v \sin i \rangle_{\text{line}}$ yields a varied range of correlations what can be said that results differs for different He I lines to measure $v \sin i$.

Despite the use of He I lines, some of this variety of results could be due to the contamination of the disc to observe the photosphere

on the stars. More studies in CBes, or massive high rotator stars, should be done at different epochs regarding the structure of a disc at different epochs to study if effectively this envelope contaminate the absorption line. Another theory is that not all the He I must be distributed only on the equator, the poles, uniformly, and/or even, irregularly. Each transition could have a preferred location in the photosphere and deeper physics calculations should be done to improve this approach. Regarding to $\lambda 4437$, this line was not taken into account for the 314 spectra analysed and it is an useless absorption line to measure $v \sin i$ on CBes. This could be because is an optically thin line.

6.3 The epsilon parameter

For eq. 1 it is possible to display ε as a function of the color index $B - V (I(\cos \theta))$, i. e., proportional to the temperature (Gray 2005). The astronomical community since the work of Carroll (1928) assume a LD coefficient $\varepsilon = 0.6$ by default. This supposition is not quite true because the range of all spectral types stars, a difference of temperature is supported for separate stars. The expression of this coefficient is interpreted as an uniformly illuminated stellar disc for $\varepsilon = 0$ to a disc fully darkened for $\varepsilon = 1$. Furthermore, every single star should confine different features and is not useful to establish this value habitually. As a future work, we pretend to develop a grid of LD coefficients using non-linear models of LD laws (Wade & Rucinski 1985; Levenhagen 2014) to fit the spectrum to well-known stars.

6.4 Fast rotational effect

The classical gravity darkening theory (von Zeipel 1924a,b) describes the local dependency of temperatures and radiative fluxes

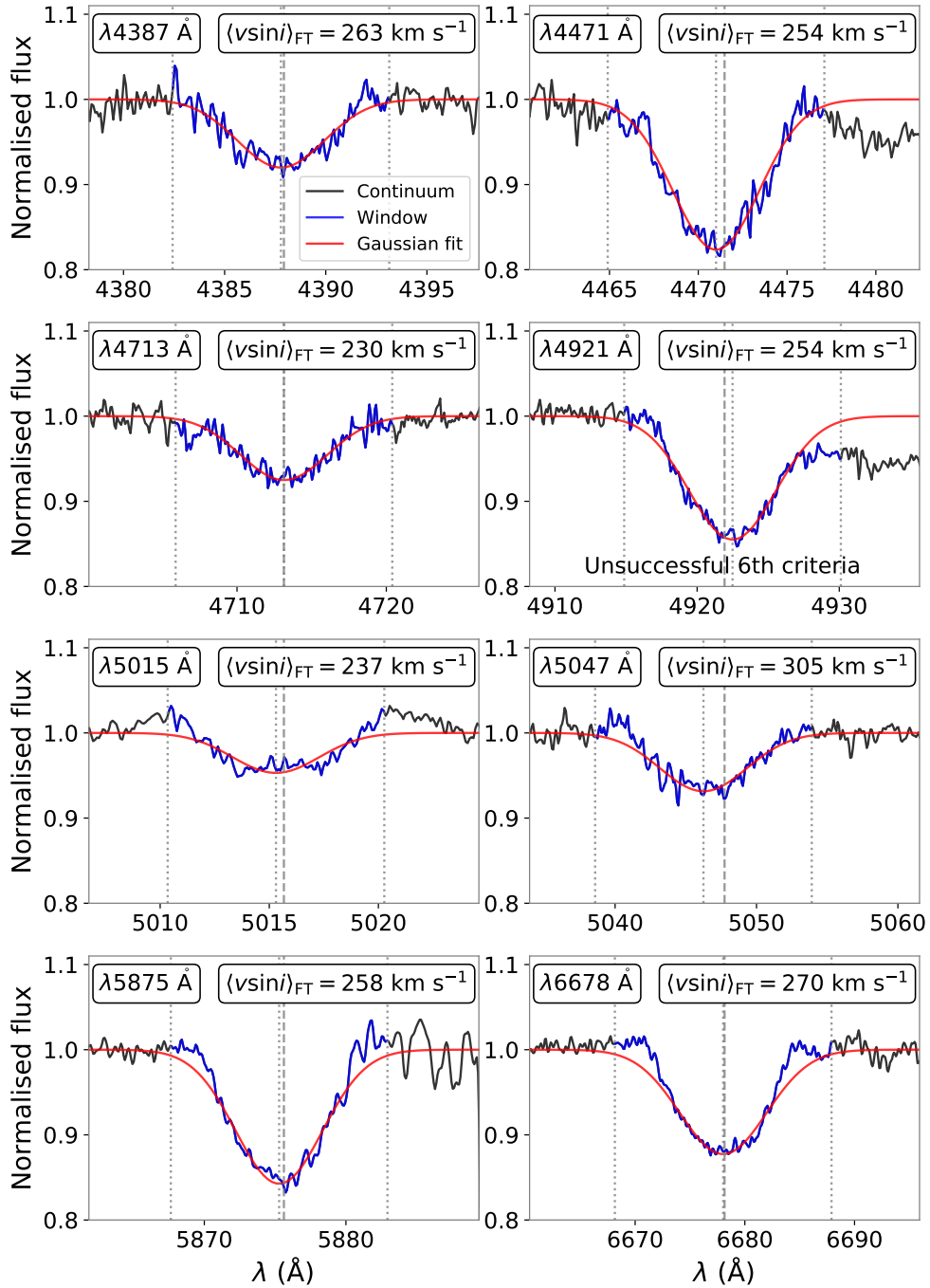


Figure 5. Procedure applied to the eight He I spectral lines in HD157246 for a window of $2.5 \sigma_{\text{fit}}$. Normalised flux as a function of wavelengths. Solid red curve represents the best Gaussian fitted, blue solid lines are the spectral signal selected and solid black lines the continuum. In the inset of each subplot the midwave and rotational speed obtained are shown. Vertical dotted grey lines represents the limit of the signal and midwave given by the Gaussian fit. Vertical dashed grey lines are the laboratory He I midwave. $\lambda 4921$ did not satisfy the sixth criterion.

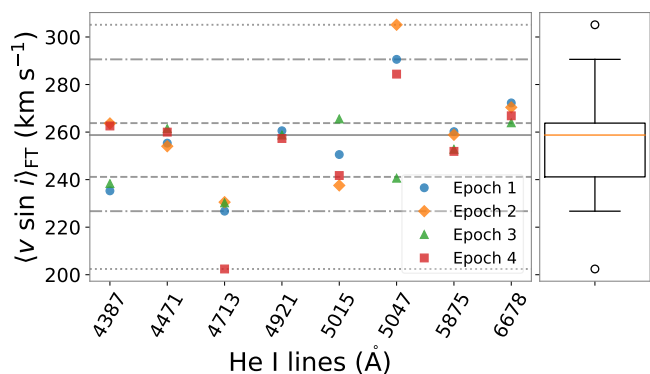


Figure 6. Projected rotational velocities obtained for HD157246 at different epochs as a function of the respective He I line. Left plot: Each symbol and colour is a specific spectrum for a unique epoch. These epochs (1 - 4) are given by 56 735.3323, 57 078.3089, 57 218.1718, 57 218.1793 in Modified Julian Dates, respectively. The horizontal solid, dashed, dashed-dotted and dotted grey lines gives the median, first and third quartile, minimum and maximum, and outliers, respectively. Right panel: Standard boxplot for all $v \sin i$ values given by the different epochs.

with the fractional radius of the star, which is dependent on the colatitude for a fast spinning star and gives rise to an oblate geometry (Harrington & Collins 1968). Although sounding reasonable, a detailed examination of the classical von Zeipel’s equation results in a problem known as the von Zeipel’s paradox (Zorec et al. 2017), where stellar layers outside the stellar core present nonzero divergence of the radiative flux that gives rise to meridional circulations known as Eddington-Sweet currents (Tassoul 2007). Further improvements to the theory were proposed (Espinosa Lara & Rieutord 2011; Zorec et al. 2017) leading to a different structure of fractional radii and a different dependence of temperatures and radiative fluxes with the stellar colatitude.

Our FT analysis in this work considers spherical shapes and rigid rotation, neglecting subtle GD and geometrical deformation. It is worth emphasising that previous works revealed that projected rotational velocities measured from the fittings of classical model atmospheres or even FT techniques are indeed apparent quantities if these effects are not considered, leading possibly to $v \sin i$ underestimations (Stoeckley 1968; Townsend et al. 2004; Zorec et al. 2016, 2017). In order to figure out, to some extent, the difference between classical FT estimations and models accounting for GD, we performed fittings of GD models to the observed stellar spectra using a code to account for the classical von Zeipel’s effect (ZPEKTR; Levenhagen 2014; Levenhagen et al. 2021). The apparent $v \sin i$ values were estimated with FT with a spectral window size of $3.0 \sigma_{\text{fit}}$ (Fig. 9). The expected “true” $v \sin i$ values were derived through the use of correction factors δT_{eff} , $\delta \log g$ and $\delta v \sin i$ by Frémat et al. (2005) to the averaged GD parameters obtained during the fitting procedures with ZPEKTR.

As can be noticed in the figure, modelling GD effects yield higher values and this is more considerable for velocities higher than 100 km s^{-1} . Along with this result, a linear fit is computed to quantify how is the behaviour for this overestimation. The linear fit for $v \sin i$ with GD versus without GD is given by $y = 1.111x - 2.013$ yielding a clearly underestimation of $\sim 10 \%$ for projected rotational speeds when GD effects are not taken into account. Confidence and prediction limits are also shown.

7 CONCLUSIONS

Stellar rotation is a fundamental parameter to constrain models of stellar formation and evolution. There is a wide field of research regarding stellar rotation: evolution and internal mechanism, GD, differential rotation, magnetic fields, angular momentum, convection/radiation energy transport, stellar oscillations, chemical mixing, mass-loss, rotation braking, among others (Meynet & Maeder 2000). In this work we presented a new procedure for the automatic $v \sin i$ estimation of fast rotating Be-type stars. This procedure, based on the FT method proposed by Carroll (1933), showed to be suitable for stars with $v \sin i > 50 \text{ km s}^{-1}$ using a high-resolution instrument of $R \sim 65000$ (Sundqvist et al. 2013).

As Doppler effect broad intrinsic line profiles in atomic transitions for rotating stars, it is possible to measure $v \sin i$ data via FT technique in high rotator stars (not only CBe) since broadening of lines are mainly dominated by rotation being the other effects neglectable, as microturbulence, macroturbulence, instrumental errors, among others. We performed a procedure that gives the $v \sin i$ value for any selected absorption line profiles. In our case, the photosphere of CBes, are the lines He I $\lambda\lambda 4387, 4471, 4713, 4921, 5015, 5047, 5875$ and 6678 . A Gaussian profile is fitted to the absorption line to select automatically the signal. The dispersion parameter of this Gaussian fit, σ_{fit} , is used to determine the different window sizes by $k \sigma_{\text{fit}}$.

We perform MC simulations for a grid of velocities (100 to 600 in steps of 10 km s^{-1}) and synthetic Normal noise added (0.001 to 0.1 in steps of 0.001 from pseudo-random dispersion parameter). The MC simulations forced the foundation for a new sixth criteria in which it is necessary to measure the standard deviation of the continuum and if it is higher than a threshold from Fig. 3 therefore is not considered as a “good” line and is dropped.

The procedure was applied to BeSOS database for 64 stars at different epochs with a total of 314 spectra. The results are in global agreement in comparison to Arcos et al. (2018) and Frémat et al. (2005), with the main difference that our method includes an average for eight He I lines at different epochs. The importance of develop an automatic algorithm yields in the research field of Big Data Era and the fact that this method can include any midwave, being our case these eight He I lines, a more detailed statistic research could be done for rotational velocities in high rotators and/or, even so, slow rotators at high resolution spectra for large databases. This study would conceive a new branch of the astrophysics in stellar rotations.

As He I $\lambda 4471$ is the most common absorption line to measure $v \sin i$ in CBes (Zorec et al. 2016), we have extended the survey by analysing other He I lines: $\lambda\lambda 4387, 4471, 4713, 4921, 5015, 5047, 5875$ and 6678 . In summary, measuring the FT signal for different lines gives non-similar values.

For a complete study, non-linear solutions should be taken into account using a grid of limb-darkening coefficients to simulate the rotation profiles of stellar photospheres. Also, effects of gravity darkening need to be included (Frémat et al. 2005; Zorec et al. 2017) since for fast rotators, the emerging flux from equatorial regions are reduced as the local gravity in these regions are small, which leads to the underestimation of $v \sin i$. We plan to employ the ZPEKTR code (Levenhagen 2014) to include the classical GD effects and also the Espinosa-Lara’s scheme (Espinosa Lara & Rieutord 2011) for high rotating stars in further studies.

ACKNOWLEDGEMENTS

M.S. acknowledges grant support from project Beca de Magíster Nacional 2020, ANID (ex Conicyt), folio 22200219. M.C. and C.A. ac-

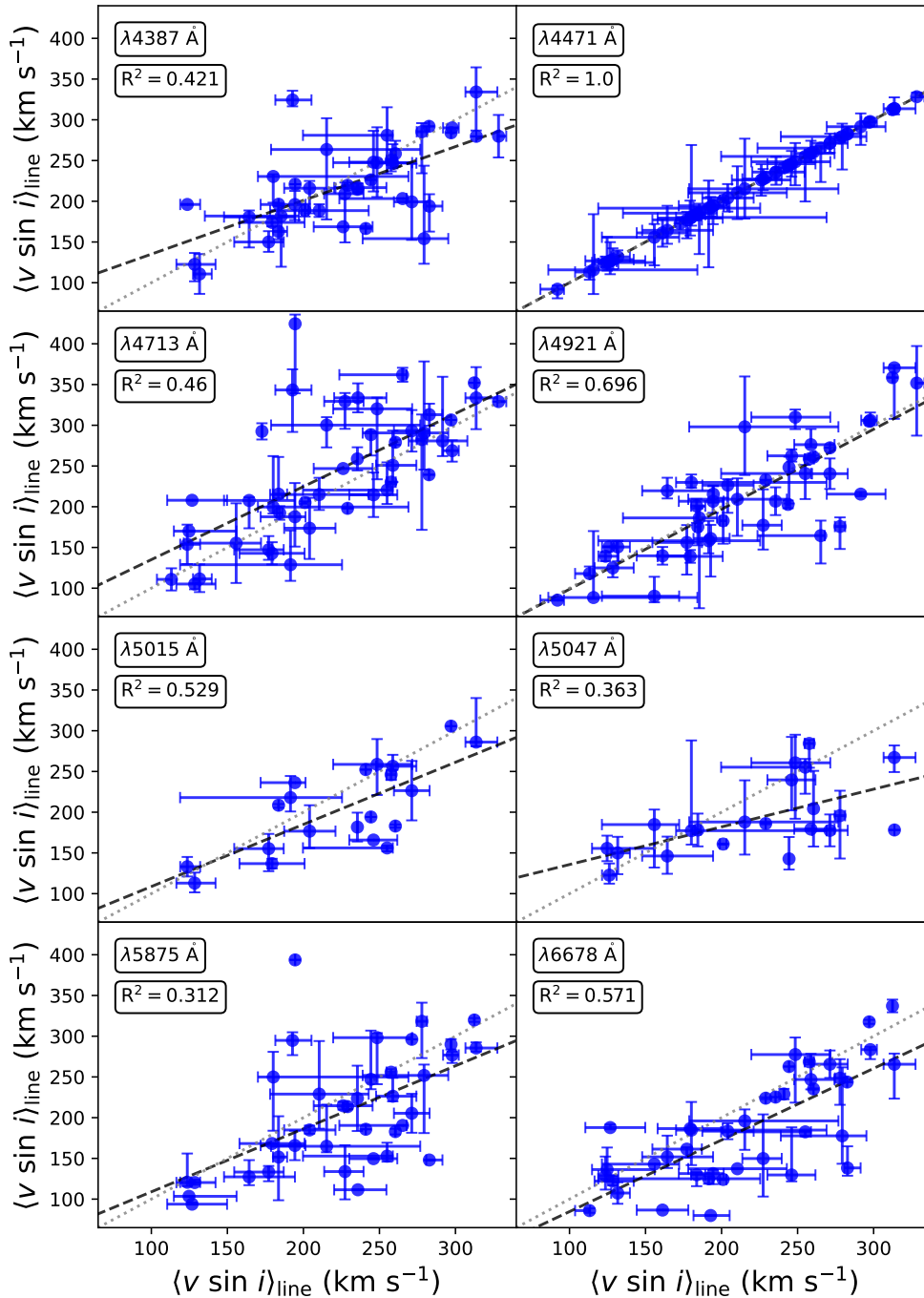


Figure 7. Final $v \sin i$ averaged per line ($\langle v \sin i \rangle_{\text{line}}$) as a function of $\langle v \sin i \rangle_{\text{line}}$ for He I $\lambda 4471$ using a window of $2.5 \sigma_{\text{fit}}$ (black dots). Error bars are given by a 16% – 84% confidence interval. In the inset of each plot the He I lines and the correlation coefficient squared are represented. The dashed black line are the least square polynomial fit. The 1:1 relation is also showed (dashed grey line).

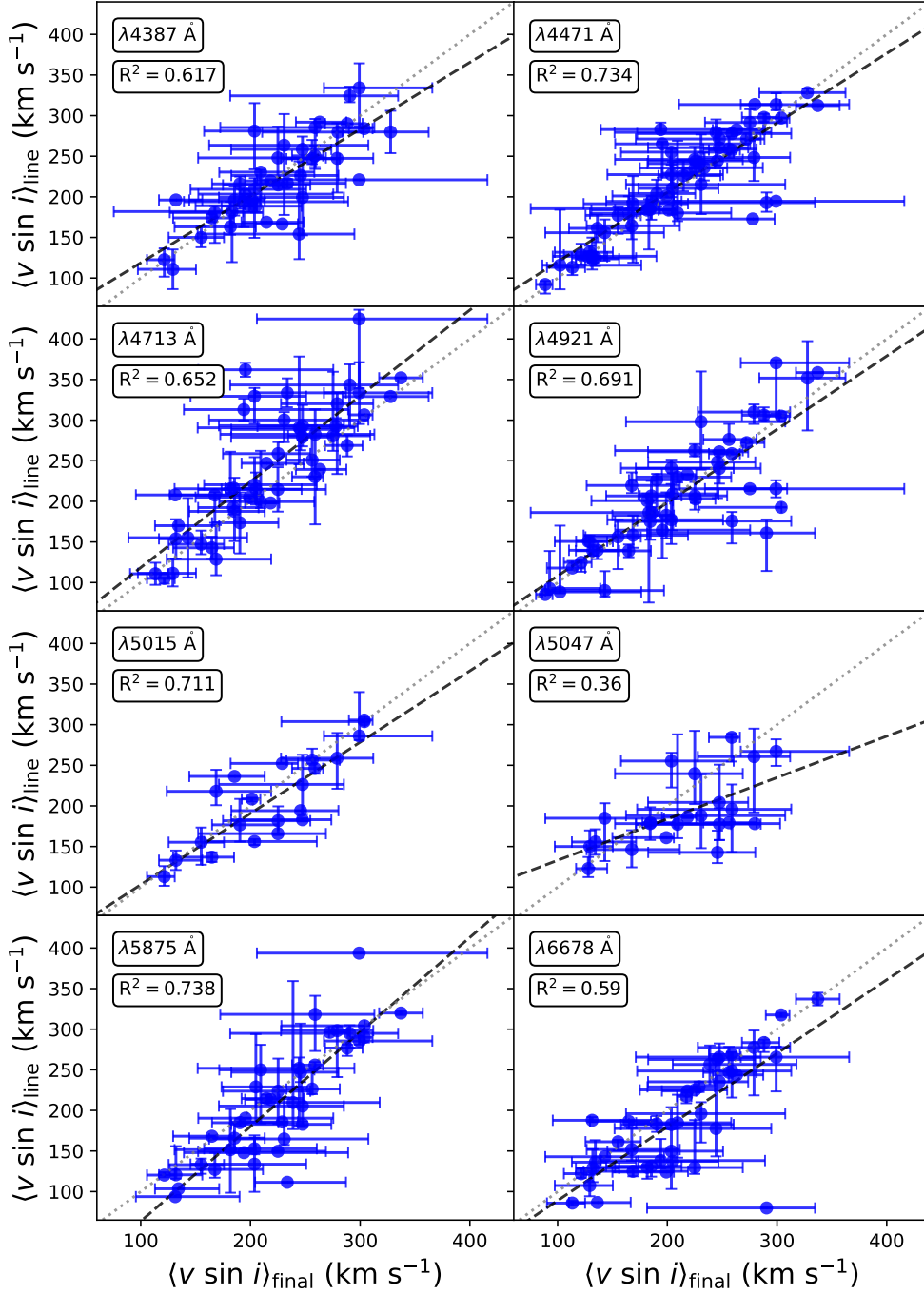


Figure 8. $\langle v \sin i \rangle_{\text{line}}$ as a function of the final $v \sin i$ averaged for the star using all He I lines ($\langle v \sin i \rangle_{\text{final}}$) with a window of $2.5\sigma_{\text{fit}}$ (black dots). Error bars are given by a 16% – 84% confidence interval. In the inset of each plot the He I lines and the correlation coefficient squared are represented. The dashed black line are the least square polynomial fit. The 1:1 relation is also showed (dashed grey line).

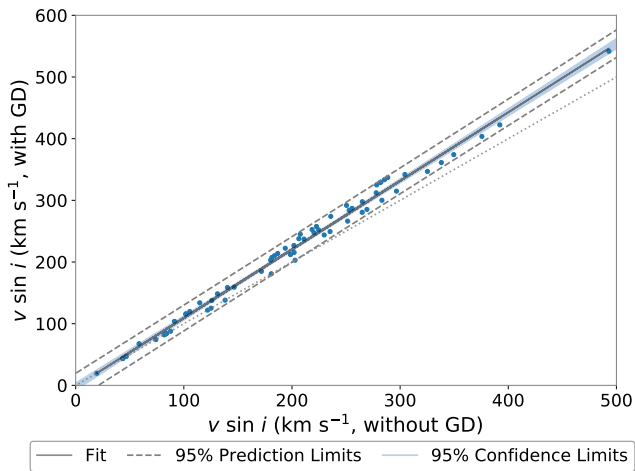


Figure 9. $v \sin i$ using GD as a function of $v \sin i$ without GD models (blue dots). The dotted grey line is a 1:1 relation.

knowledges partial support from Centro de Astrofísica de Valparaíso. MC also acknowledge support from Centro Interdisciplinario de Estudios Atmosféricos y Astroestadística, Universidad de Valparaíso. This work used BeSOS Catalogue, operated by the Instituto de Física y Astronomía, Universidad de Valparaíso, Chile: <http://besos.ifa.uv.cl> and funded by Fondecyt iniciación N° 11130702. C.A. thanks to FONDECYT N° 11190945. C.A., M.C. and I.A. thank the support from FONDECYT project N.1130485. I.A. thanks the support from FONDECYT project 11190147. M.S., M.C. I.A. and C.A. thank to project ANID-FAPESP N°133541. This work has been possible thanks to the use of AWS-U.Chile-NLHPC credits. Powered@NLHPC: This research was partially supported by the super-computing infrastructure of the NLHPC (ECM-02). This project has received funding from the European Union’s Framework Programme for Research and Innovation Horizon 2020 (2014-2020) under the Marie Skłodowska-Curie Grant Agreement No. 823734.

Softwares: MATPLOTLIB (Hunter 2007), ASTROML (VanderPlas et al. 2012), ZPEKTR (Levenhagen 2014), ASTROPY (Astropy Collaboration et al. 2018), SciPY (Virtanen et al. 2020)

DATA AVAILABILITY

The data underlying this article will be shared on request to the corresponding author

REFERENCES

- Abney W. D. W., 1877, *MNRAS*, **37**, 278
- Arcos C., Kanaan S., Chávez J., Vanzi L., Araya I., Curé M., 2018, *MNRAS*, **474**, 5287
- Astropy Collaboration et al., 2018, *AJ*, **156**, 123
- Baade D., et al., 2016, *A&A*, **588**, A56
- Brahm R., Jordán A., Espinoza N., 2017, *PASP*, **129**, 034002
- Bruning D. H., 1981, *ApJ*, **248**, 274
- Carroll J. A., 1928, *MNRAS*, **88**, 548
- Carroll J. A., 1933, *MNRAS*, **93**, 478
- Carroll J. A., Ingram L. J., 1933, *MNRAS*, **93**, 508
- Collins George W. I., Truax R. J., 1995, *ApJ*, **439**, 860
- Díaz C. G., González J. F., Levato H., Grosso M., 2011, *A&A*, **531**, A143
- Dravins D., Lindegren L., Torkelson U., 1990, *A&A*, **237**, 137
- Espinosa Lara F., Rieutord M., 2011, *A&A*, **533**, A43
- Frémat Y., Zorec J., Hubert A. M., Floquet M., 2005, *A&A*, **440**, 305
- Gaia Collaboration et al., 2021, *A&A*, **649**, A1
- Gray D. F., 1977, *ApJ*, **211**, 198
- Gray D. F., 2005, *The Observation and Analysis of Stellar Photospheres*. Cambridge University Press
- Harrington J. P., Collins George W. I., 1968, *ApJ*, **151**, 1051
- Hubeny L., Lanz T., 1995, *ApJ*, **439**, 875
- Hunter J. D., 2007, *Computing in Science and Engineering*, **9**, 90
- Ilin V. B., Ivanov V. V., 1979, *Soviet Astronomy Letters*, **5**, 152
- Jankov S., 1995, *Publications de l’Observatoire Astronomique de Beograd*, **50**, 75
- Kaufer A., Stahl O., Tubbesing S., Nørregaard P., Avila G., Francois P., Pasquini L., Pizzella A., 1999, *The Messenger*, **95**, 8
- Kopal Z., 1950, *Harvard College Observatory Circular*, **454**, 1
- Kurucz R. L., 1979, *ApJS*, **40**, 1
- Levenhagen R. S., 2014, *ApJ*, **797**, 29
- Levenhagen R. S., Diaz M. P., Amôres E. B., Leister N. V., 2021, *MNRAS*, **501**, 747
- Maeder A., Meynet G., 2010, *New Astronomy Reviews*, **54**, 32
- Meynet G., Maeder A., 2000, *A&A*, **361**, 101
- Mihalas D., 1964, *ApJ*, **140**, 885
- Neiner C., et al., 2002, *A&A*, **388**, 899
- O’Mara B. J., Simpson R. W., 1972, *A&A*, **19**, 167
- Porter J. M., Rivinius T., 2003, *PASP*, **115**, 1153
- Preston G. W., Sneden C., Chadid M., Thompson I. B., Sheckman S. A., 2019, *AJ*, **157**, 153
- Ramírez-Agudelo O. H., et al., 2013, *A&A*, **560**, A29
- Reiners A., 2003, *A&A*, **408**, 707
- Reiners A., Schmitt J. H. M. M., 2002, *A&A*, **384**, 155
- Rivinius T., Carciofi A. C., Martayan C., 2013, *A&ARv*, **21**, 69
- Royer F., 2005, *Memorie della Societa Astronomica Italiana Supplementi*, **8**, 124
- Shajn G., Struve O., 1929, *MNRAS*, **89**, 222
- Simón-Díaz S., Herrero A., 2007, *A&A*, **468**, 1063
- Simón-Díaz S., Herrero A., 2014, *A&A*, **562**, A135
- Simón-Díaz S., Herrero A., Esteban C., Najarro F., 2006, *A&A*, **448**, 351
- Skrutskie M. F., et al., 2006, *AJ*, **131**, 1163
- Slettebak A., 1954, *ApJ*, **119**, 146
- Slettebak A., 1955, *ApJ*, **121**, 653
- Slettebak A., 1956, *ApJ*, **124**, 173
- Slettebak A., Howard R. F., 1955, *ApJ*, **121**, 102
- Slettebak A., Collins G. W. I., Boyce P. B., White N. M., Parkinson T. D., 1975, *ApJS*, **29**, 137
- Smith M. A., Gray D. F., 1976, *PASP*, **88**, 809
- Stoeckley T. R., 1968, *MNRAS*, **140**, 141
- Sundqvist J. O., Simón-Díaz S., Puls J., Markova N., 2013, *A&A*, **559**, L10
- Tassoul J.-L., 2007, *Stellar Rotation*
- Tody D., 1993, in Hanisch R. J., Brissenden R. J. V., Barnes J., eds, *Astronomical Society of the Pacific Conference Series Vol. 52, Astronomical Data Analysis Software and Systems II*. San Francisco, Calif. : Astronomical Society of the Pacific, p. 173
- Townsend R. H. D., Owocki S. P., Howarth I. D., 2004, *MNRAS*, **350**, 189
- VanderPlas J., Connolly A. J., Ivezić Z., Gray A., 2012, in *Proceedings of Conference on Intelligent Data Understanding (CIDU)*. pp 47–54 ([arXiv:1411.5039](https://arxiv.org/abs/1411.5039)), doi:10.1109/CIDU.2012.6382200
- Vanzi L., et al., 2012, *MNRAS*, **424**, 2770
- Vinicius M. M. F., Zorec J., Leister N. V., Levenhagen R. S., 2006, *A&A*, **446**, 643
- Virtanen P., et al., 2020, *Nature Methods*, **17**, 261
- Wade R. A., Rucinski S. M., 1985, *A&AS*, **60**, 471
- York D. G., et al., 2000, *AJ*, **120**, 1579
- Zorec J., et al., 2016, *A&A*, **595**, A132
- Zorec J., et al., 2017, *A&A*, **602**, A83
- von Zeipel H., 1924a, *MNRAS*, **84**, 665
- von Zeipel H., 1924b, *MNRAS*, **84**, 684

APPENDIX A: VELOCITIES OBTAINED IN OUR WORK COMPARED WITH LITERATURE

In order to compare the values of Table 2, in Fig. A1 there is shown the relation of these results.

In general terms, it can be inferred that for slow rotators ($\lesssim 200 \text{ km s}^{-1}$) our values overestimate the ones from Arcos+2018 and Fremat2005 and for high rotators ($\gtrsim 200 \text{ km s}^{-1}$) our values are underestimated, where if GD effects are taken into account then the results are improved.

This paper has been typeset from a $\text{\TeX}/\text{\LaTeX}$ file prepared by the author.

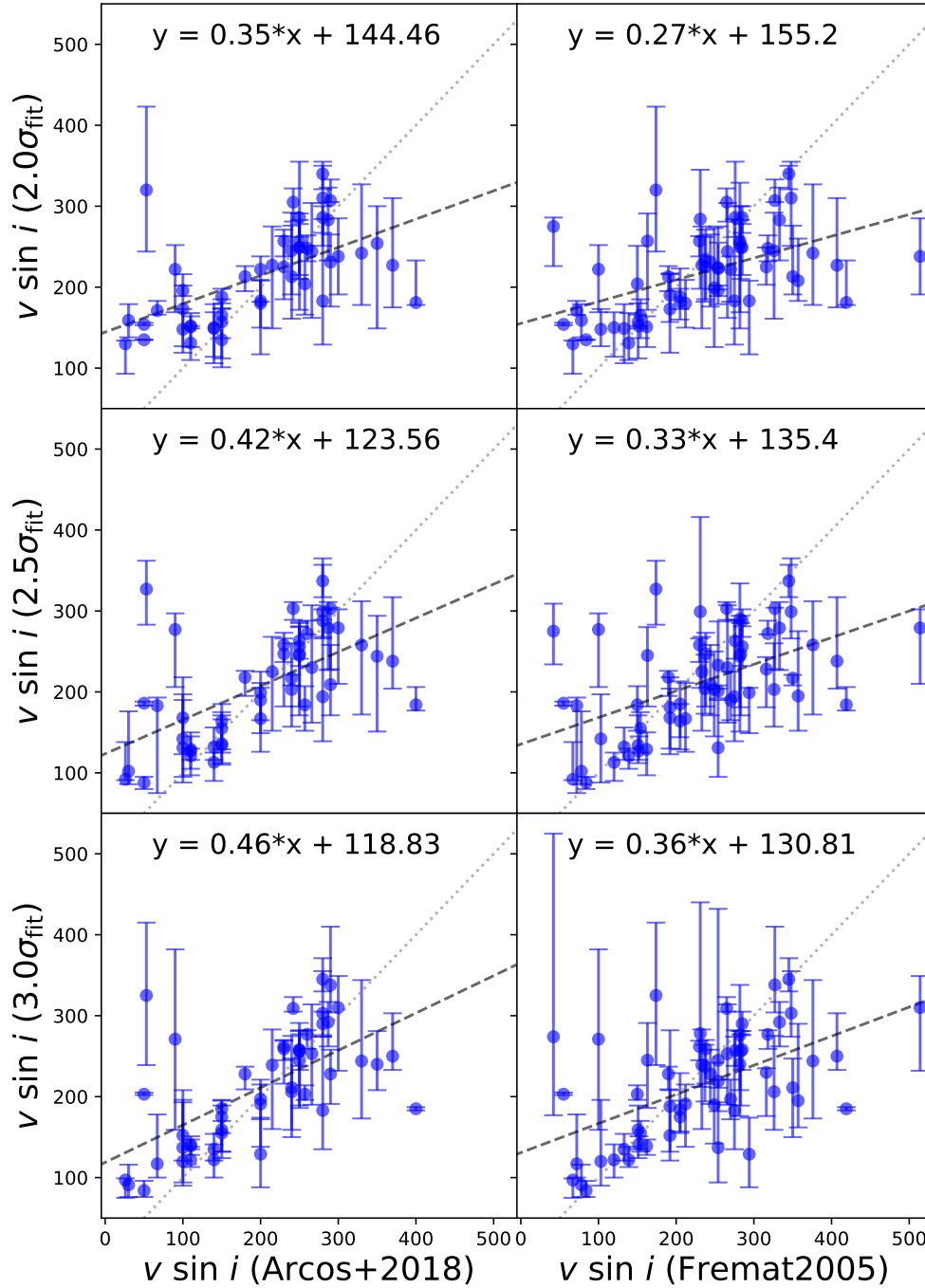


Figure A1. $v \sin i$ values obtained by our method (errorbars are percentile 16th and 84th) as a function of projected rotational velocities literature results in blue dots. Top, middle and bottom panels are for $k = 2.0, 2.5$ and 3.0 window sizes, respectively. Left and right panels corresponds to Arcos+2018 and Fremat2005, respectively. Dashed black and dotted grey lines are the linear fit to dots and 1:1 relation.